

Vibration of induction motor rotor in rotating magnetic field (Case of two-pole motor)

著者	Iwata Yoshio, Sato Hidenori, Komatsuzaki Toshihiko, Saito Takuhiro
journal or publication title	JSME International Journal, Series C: Mechanical Systems, Machine Elements and Manufacturing
volume	44
number	3
page range	603-609
year	2001-09-01
URL	http://hdl.handle.net/2297/17056

doi: 10.1299/jsmec.44.603

Vibration of Induction Motor Rotor in Rotating Magnetic Field*

(Case of Two-Pole Motor)

Yoshio IWATA**, Hidenori SATO**,
Toshihiko KOMATSUZAKI** and Takuhiro SAITO***

The rotor vibration of two-pole induction motor with rotating magnetic field has been investigated. The vibration is measured at any relative location of the stator and the rotor with various power supply frequencies in the experiment and is analyzed in consideration of mechanical factors of the rotor. The following conclusion is obtained through the experiment and the analysis; (1) 2ω vibration of twice the power supply frequency ω is generated because of offset between the stator center and the gyrational center of the rotor. (2) Two vibrations of $\omega(1-s)$ and $\omega(1+s)$ where s is slip ratio are generated because of the rotor unbalance or the disagreement between the gyrational center and geometrical center of the rotor. (3) An unstable vibration is predicted in the analysis when the power supply frequency is equal to natural frequency of the rotor, however, the unstable vibration was not generated in the experiment because of the damping.

Key Words: Vibration of Rotating Body, Electromagnetic Induced Vibration, Parametric Excitation, Induction Motor, Rotating Magnetic Field, Magnetic Pull Force

1. Introduction

Bending vibrations in rotor of an induction motor are caused by the rotor unbalance and the magnetic pull force of the stator, along with various types of vibration which are related to various motor conditions⁽¹⁾. It is known that unstable vibration^{(2),(3)} equal to the power supply frequency, vibration of twice the power supply frequency⁽⁴⁾, beat vibration concerning with slip ratio of rotation⁽⁵⁾ etc., are generated regardless of the rotor unbalance, which are due to the magnetic factor of three-phase two-pole induction motor, offset between the stator center and a gyrational center of the rotor, imbalance of the stator magnetic force and unbalanced phase voltage. Studies

exclude unstable vibrations have been reported where the vibration is simply explained by electromagnetic property of magnetic pull force between the stator and the rotor, however, it does not seem to be fully analyzed in rotordynamic aspects for the present rotor system.

In this paper, the various bending vibrations of the rotor in three-phase two-pole induction motor, which is often applied to large induction motor are reported. The three-phase induction motor whose rotor is driven by rotating magnetic field in the stator is assumed to have the ideal rotating magnetic field without magnetic imbalance or magnetic deformation, and then we investigated the vibration which is related to mechanical factor of the rotor such as offset between the stator center and the gyrational center of the rotor, disagreement between the gyrational center and a geometrical center of the rotor. By reversely utilizing this result, it is expected to be able to specify the cause of vibration in the induction motor.

2. Experiment

2.1 Experimental procedure

The rotor vibration in a single-phase two-pole

* Received 24th November, 2000. Japanese original: Trans. Jpn. Soc. Mech. Eng., Vol. 65, No. 638, C (1999), pp. 3919-3925 (Received 20th January, 1999)

** Department of Human and Mechanical Systems Engineering, Kanazawa University, 2-40-20 Kodatsuno, Kanazawa 920-8667, Japan. E-mail: iwata@t.kanazawa-u.ac.jp

*** Nissei Build Corp., 3-16-10 Kanaiwakita, Kanazawa 920-0396, Japan

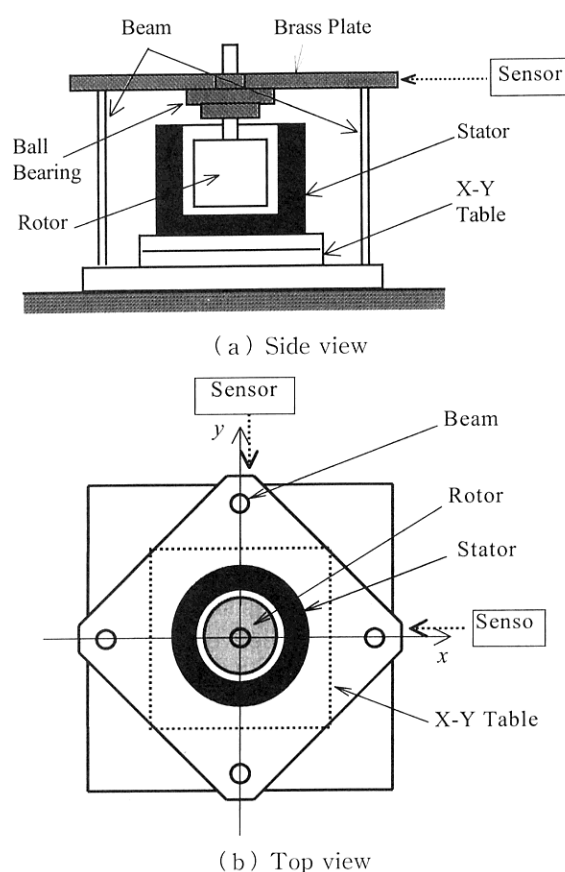


Fig. 1 Experimental equipment

induction motor was investigated experimentally. The stator of the motor consists of a pair of primary windings and also a pair of auxiliary windings, of which magnetic fluxes are orthogonal and have phase shift of 90 degrees to each other. The magnetic field in the stator then becomes rotating field whose rotational frequency is equal to the power supply frequency, therefore, we investigated the rotor vibration in rotating magnetic field equal to power supply frequency in the experiment.

The experimental equipment is shown in Fig. 1. 40 watts single-phase two-pole induction motor was decomposed, and the rotor was separated from the stator for measuring the rotor vibration. Upper side of the rotor was supported on a brass plate by a ball bearing and the brass plate was mounted on a base by four beams with 8 mm in diameter and 120 mm in length. The brass plate is displaced in the horizontal direction by deflection of the beams, therefore the rotor vibrates in identical direction. This vibration corresponds to the bending vibration of actual induction motor rotor. The vibration of the brass plate was measured in x and y directions using non-contact eddy type displacement sensor. The stator was fixed on a bed (the x - y table) which is movable in x and y directions to set the stator location variable, hence it

is possible to change the relative location between the rotor and the stator. Because the original clearance between the stator and the rotor was very small, treatment was made for the rotor to decrease its outer diameter. As a result, outer diameter of the rotor became 34.4 mm while the inner diameter of the stator was 35.0 mm, so that the radius clearance became 0.3 mm, consequently. The amplified signal of an oscillator was supplied as a power source to the induction motor. Since the power supply frequency became variable, it was possible that the rotational speed of motor magnetic field was optionally set. The natural frequencies of the system which consisted of the rotor, the brass plate and the four beams were observed at 82.5 Hz in both x and y directions. However, the time trace of free vibration showed that the damping of x direction was larger than that of y direction.

In this experiment, the vibration spectrum in respective x and y directions was measured at each power supply frequency set to every 5 Hz step from 25 Hz to 85 Hz, where the relative location of the rotor and the stator was variously changed. This relative location was arranged based on a reference location of the stator, where the vibration of rotationally restricted rotor becomes the smallest. It is because the rotor located at the stator center does not vibrate, since the magnetic pull force from the stator is balanced at that position. The stator was moved to negative x direction every 0.1 mm distance and the rotor vibration was measured respectively. It is equal to what the rotor would be relatively moved to positive x direction, hence we consider moving of the rotor location instead of the stator in the following sections. Furthermore, the amplification factor for AC power supply of induction motor was fixed in all experiment, therefore the input AC value to the motor was dependent on the source frequency. Though it was possible to adjust the amplified AC voltage become constant, however, it often caused instability in motor behavior.

2.2 Experimental result

Vibration of the rotor operated on the reference position was measured in both x and y directions, and whose results are shown in Fig. 2(a) and 2(b), respectively. Also Fig. 3(a) and 3(b) show experimental results in respective directions where the rotor location was set to 0.2 mm distant from the reference position. Here, we omitted the case of 0.1 mm, which showed similar results with 0.2 mm. Figures 2 and 3 illustrate spectrum distribution in three-dimensional form for up to 200 Hz at each power supply frequency. In the case where the component of vibration response has the same characteristics, a solid line is drawn on the side of peaks and also the letters ω_1 , ω_2 , $2\omega_1$ and $2\omega_2$

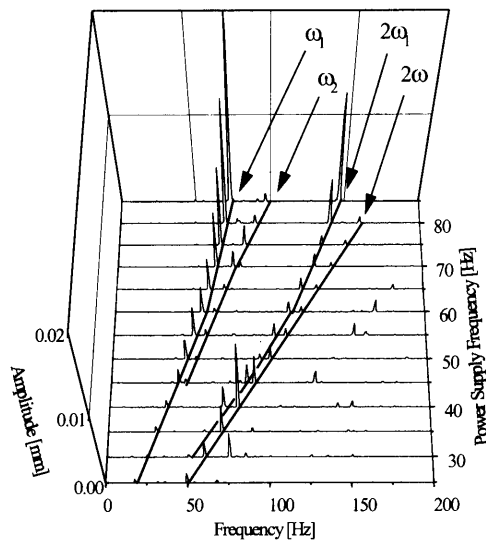
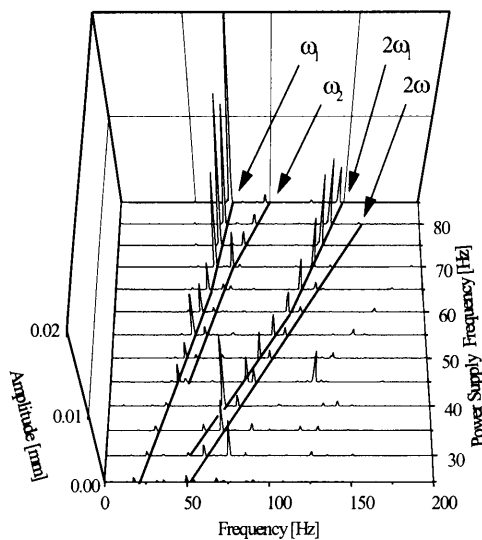
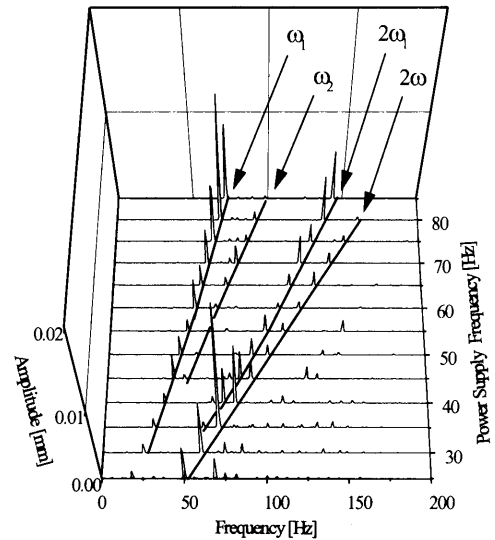
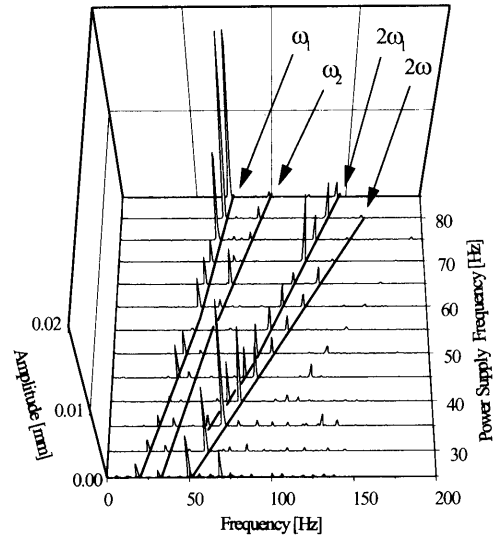
(a) *x* direction(b) *y* direction

Fig. 2 Experimental result (reference position)

were added. Those letters represent vibration components, which are explained as follows:

ω_1 shows the rotational speed of the rotor expressed as $\omega_1 = \omega(1-s)$, where ω represents rotational speed of rotating magnetic field and s represents slip ratio of the induction motor. The ω_1 component was most eminently generated through all the experiments. ω_2 is expressed similarly as $\omega_2 = \omega(1+s)$. $2\omega_1$ shows twice the rotational speed ω_1 and 2ω twice the rotational speed ω of rotating magnetic field. The ω_1 component extremely increases as the speed of rotating magnetic field approaches to the natural frequency (about 80 Hz), however, the amplitude over 0.02 mm is not displayed in the figure because of the appropriate range for convenience. The other ω_2 , $2\omega_1$ and 2ω components also become large in the vicinity where each component agrees with the natural frequency. It

(a) *x* direction(b) *y* directionFig. 3 Experimental result (0.2 mm offset in *x*-direction from reference position)

is found by comparison between Fig. 2 and Fig. 3 that 2ω component becomes large as the distance of the rotor location increases, while the other components are not dependent on the distance. Although the rotor was moved only in the *x* direction, 2ω component increases in both *x* and *y* directions simultaneously.

Figure 4 shows the slip ratio s , which is obtained from a difference between the power supply frequency and the rotational speed of the rotor. The slip ratio is minimized when the power supply frequency ranges from 50 - 60 Hz near the rated operating speed, and also increases rapidly and rather slowly at the frequency less than 45 Hz and over 60 Hz, respectively. Every solid line shown in Fig. 2 and Fig. 3, which corresponds to components ω_1 , ω_2 and $2\omega_1$ are not a straight line because the slip ratio is dependent on the

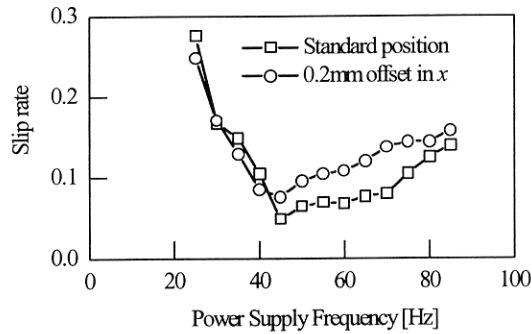


Fig. 4 Slip rate

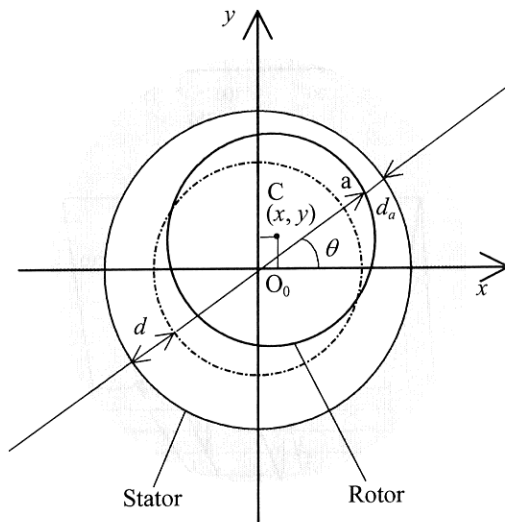


Fig. 5 Stator and rotor

power supply frequency.

3. Vibration Analysis of Rotor

3.1 Magnetic pull force

Figure 5 shows geometry and coordinate system used in the analysis, where O_0 is placed at the stator center. The mathematical formulations are derived for the magnetic pull force when the geometrical center C of the rotor is located at coordinate (x, y) . In the present analysis we followed conventional method, which is practically used for induction motor design. Gap d_a between the rotor and the stator at point a , which is located on the rotor circumference with angle θ from the x axis, is given by

$$d_a = d - x \cos \theta - y \sin \theta \quad (1)$$

where d is radial clearance between the rotor and the stator. When F_a , B_a and μ_0 are the magnetic pull force per unit area at point a , the magnetic flux density at point a and the magnetic permeability of air gap respectively, F_a is expressed as the following equation.

$$F_a = \frac{B_a^2}{2\mu_0} \quad (2)$$

When B_a is assumed to be proportional to the recipro-

cal of gap ratio d_a/d with the proportionality constant B_0 which is the magnetic flux density at $x=0$ and $y=0$, F_a is given as follows.

$$F_a = \frac{1}{2\mu_0} \left(\frac{d}{d_a} B_0 \right)^2 \quad (3)$$

Then, x and y components of F_a are represented as follows.

$$\begin{cases} F_{ax} = F_a \cos \theta \\ F_{ay} = F_a \sin \theta \end{cases} \quad (4)$$

The x and y components of the magnetic pull force between the rotor and the stator, F_x and F_y , can be obtained by integrating Eq. (4) along the circumference of the rotor as follows,

$$\begin{cases} F_x(x, y) = \frac{d^2 RL}{2\mu_0} \int_0^{2\pi} \frac{B_0^2 \cos \theta}{(d - x \cos \theta - y \sin \theta)^2} d\theta \\ F_y(x, y) = \frac{d^2 RL}{2\mu_0} \int_0^{2\pi} \frac{B_0^2 \sin \theta}{(d - x \cos \theta - y \sin \theta)^2} d\theta \end{cases} \quad (5)$$

where R is outer radius of the rotor core and L length.

Since the rotational speed of rotating magnetic field is equal to the power supply frequency ω in two-pole induction motors, circumferential distribution of the magnetic flux density B_0 can be expressed by the following equation.

$$B_0 = B \cos(\theta - \omega t) \quad (6)$$

Although F_x and F_y can be obtained by substituting Eq. (6) into Eq. (5), the integration cannot be performed explicitly. If we based on the assumption that x and y are much smaller than d , the magnetic pull force is approximately expressed as follows.

$$\begin{cases} F_x(x, y) = \frac{\pi B^2 RL}{4\mu_0 d} (2x + x \cos 2\omega t + y \sin 2\omega t) \\ F_y(x, y) = \frac{\pi B^2 RL}{4\mu_0 d} (2y + x \sin 2\omega t - y \cos 2\omega t) \end{cases} \quad (7)$$

F_x and F_y essentially become nonlinear functions with respect to x and y , but are regarded as linear functions.

In the case of multi-pole induction motor, the circumferential distribution of magnetic flux density B_0 is given as follows,

$$B_0 = B \cos(n\theta - \omega t) \quad (8)$$

where n is the number of pairs of poles. Then, F_x and F_y are represented as the following equations.

$$\begin{cases} F_x(x) = \frac{\pi B^2 RL}{2\mu_0 d} x \\ F_y(y) = \frac{\pi B^2 RL}{2\mu_0 d} y \end{cases} \quad (9)$$

The magnetic pull force is stationary, hence only degenerates bending stiffness of the rotor.

3.2 Equation of motion

Equation of motion of the induction motor rotor is derived from Fig. 6. The point S shows a gyrational center of the rotor which coincides with the point O_1

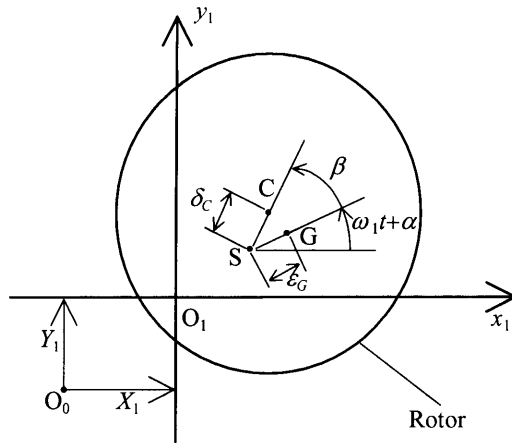


Fig. 6 Rotor location

when the rotor is static. Hence, the point O_1 denotes a static location of point S , and is located on (X_1, Y_1) away from the stator center O_0 . The point G denotes a center of gravity of the rotor which has an eccentricity ε_G to the point S . The point C indicates a geometrical center of the rotor and is located at the distance of δ_C from the point S . Those S , G and C points are respectively located on (x_s, y_s) , (x_g, y_g) and (x_c, y_c) relative to O_1 . $\omega_1 = \omega(1-s)$ shows rotational speed of the rotor, α the initial phase of the point G , and β an angle between point G and C . If we suppose that m , k and c are the mass, the bending stiffness and the viscous damping coefficient of the rotor, equation of motion of the rotor can be expressed as follows.

$$\left. \begin{aligned} m \frac{d^2 x_G}{dt^2} + c \frac{dx_s}{dt} + kx_s &= F_x(X_1 + x_c, Y_1 + y_c) \\ m \frac{d^2 y_G}{dt^2} + c \frac{dy_s}{dt} + ky_s &= F_y(X_1 + x_c, Y_1 + y_c) \end{aligned} \right\} \quad (10)$$

By substituting Eq.(7) into Eq. (10) and employing complex form with $z_G = x_G + jy_G$, $z_s = x_s + jy_s$, $z_c = x_c + jy_c$ and $z_1 = X_1 + jY_1$, the following equation is obtained.

$$\begin{aligned} m \frac{d^2 z_G}{dt^2} + c \frac{dz_s}{dt} + kz_s &= P(2z_1 + \bar{z}_1 e^{j2\omega t}) \\ &+ P(2z_c + \bar{z}_c e^{j2\omega t}) \end{aligned} \quad (11)$$

where $\bar{}$ denotes conjugate complex and $P = \pi B^2 RL / (4\mu_0 d)$. z_G and z_c can be expressed by z_s as follows.

$$z_G = z_s + \varepsilon_G e^{j(\omega_1 t + \alpha)} = z_s + \varepsilon e^{j\omega_1 t} \quad (12)$$

$$z_c = z_s + \delta_C e^{j(\omega_1 t + \alpha + \beta)} = z_s + \delta e^{j\omega_1 t} \quad (13)$$

where $\varepsilon = \varepsilon_G e^{j\alpha}$ and $\delta = \delta_C e^{j(\alpha + \beta)}$. Substituting Eq. (12) and Eq. (13) into Eq. (11) yields

$$\begin{aligned} m \frac{d^2 z_s}{dt^2} + c \frac{dz_s}{dt} + (k - 2P)z_s - P\bar{z}_s e^{j2\omega t} \\ = P(2z_1 + \bar{z}_1 e^{j2\omega t}) + m\varepsilon\omega_1^2 e^{j\omega_1 t} \\ + P(2\delta e^{j\omega_1 t} + \bar{\delta} e^{j\omega_2 t}) \end{aligned} \quad (14)$$

where $\omega_2 = \omega(1+s)$.

Eq. (14) is transformed into the following non-

dimensional form in order to investigate qualitative characteristics of the rotor vibration.

$$\begin{aligned} \frac{d^2 z}{d\tau^2} + 2\zeta \frac{dz}{d\tau} + (1 - 2\gamma)z - \gamma\bar{z} e^{j2\Omega\tau} \\ = \gamma(2Z_1 + \bar{Z}_1 e^{j2\Omega\tau}) \\ + \Omega_1^2 e^{j\alpha} e^{j\Omega_1\tau} + \gamma(2\Delta e^{j\Omega_1\tau} + \bar{\Delta} e^{j\Omega_2\tau}) \end{aligned} \quad (15)$$

where,

$$\left. \begin{aligned} z &= \frac{z_s}{\varepsilon_G}, Z_1 = \frac{z_1}{\varepsilon_G}, \Delta = \frac{\delta}{\varepsilon_G}, \zeta = \frac{c}{2\sqrt{mk}}, \gamma = \frac{P}{k} = \frac{\pi B^2 RL}{4\mu_0 dk}, \\ \omega_n &= \sqrt{\frac{k}{m}}, \tau = \omega_n t, \Omega = \frac{\omega}{\omega_n}, \Omega_1 = \frac{\omega_1}{\omega_n} = \Omega(1-s), \\ \Omega_2 &= \frac{\omega_2}{\omega_n} = \Omega(1+s) \end{aligned} \right\} \quad (16)$$

γ is a non-dimensional parameter proportional to the magnetic pull force and is considered as small in general. ζ , Ω and z are non-dimensional parameters related to damping, the power supply frequency and the vibration displacement, respectively. Each term on the right side of Eq. (15) represents external force caused by the static offset Z_1 between the stator center O_0 and the gyrational center of the rotor O_1 , the rotor unbalance, and the disagreement Δ between the gyrational and the geometrical center of the rotor. Therefore, the rotor vibration is caused by the unbalance, Z_1 and Δ .

3.3 Analytical result

First of all, we consider the case where the right side of Eq. (15) is zero, thus the case for free vibration. The same solution can be obtained as the free vibration of asymmetrical shaft, so that the following fact is available by the known result⁽⁶⁾. There is a region where the unstable vibration is generated in the vicinity of the power supply frequency equal to the natural frequency, that is, $\Omega = \sqrt{1 - 2\gamma}$. This region becomes wider with increase of γ , and becomes narrower with increase of ζ . The natural frequency decreases with increase of γ , which means that the stiffness of the rotor apparently becomes smaller due to the magnetic pull force.

Next, the excitation force term in the right side of Eq. (15) is considered. After the response for each force term is obtained, the response for all excitation can be determined according to the principle of superposition because of linearity of the equation.

When Z_1 is only considered, the equation of motion is given as follows.

$$\begin{aligned} \frac{d^2 z}{d\tau^2} + 2\zeta \frac{dz}{d\tau} + (1 - 2\gamma)z - \gamma\bar{z} e^{j2\Omega\tau} \\ = \gamma(2Z_1 + \bar{Z}_1 e^{j2\Omega\tau}) \end{aligned} \quad (17)$$

The following solution can be obtained from Eq. (17).

$$z = A_1 + A_2 e^{j2\Omega\tau} \quad (18)$$

Substituting Eq. (18) into Eq. (17), comparing each

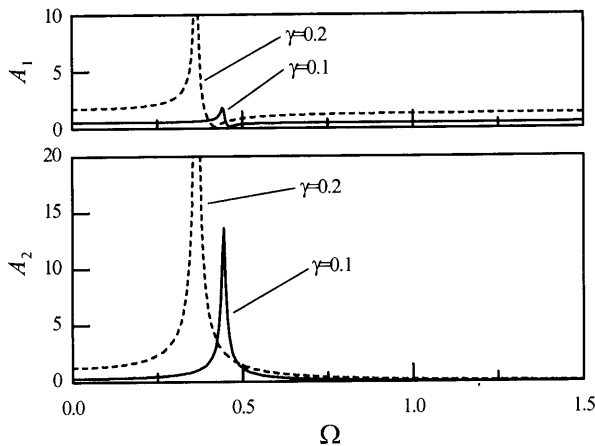


Fig. 7 Response curves of A_1 and A_2 ($Z_1=2$, $\zeta=0.01$)

corresponding constant term and coefficient of $e^{j2\Omega\tau}$ term on both sides of equation, the following equations are obtained.

$$\begin{cases} (1-2\gamma)A_1 - \gamma\bar{A}_2 = 2\gamma Z_1 \\ -\gamma\bar{A}_1 + (1-2\gamma-4\Omega^2+j4\zeta\Omega)A_2 = \gamma\bar{Z}_1 \end{cases} \quad (19)$$

A_2 which is amplitude of 2Ω component can be determined as follows.

$$A_2 = \frac{Z_1\gamma/(1-2\gamma)}{(1-4\gamma+3\gamma^2)/(1-2\gamma)-4\Omega^2+j4\zeta\Omega} \quad (20)$$

It is found from Eq.(20) that the resonance behavior would appear in the vicinity of $\Omega = \sqrt{1-2\gamma}/2$ for very small γ , and also that A_2 is proportional to Z_1 . Figure 7 shows response amplitude of A_1 and A_2 vs. Ω for two cases of $\gamma=0.1$ and $\gamma=0.2$ with respect to $Z_1=2$ and $\zeta=0.01$. The magnitude of peaks seen in A_1 and A_2 become larger with increase of γ .

When the unbalance Δ are considered, the equation of motion can be written as follows.

$$\frac{d^2 z}{d\tau^2} + 2\zeta \frac{dz}{d\tau} + (1-2\gamma)z - \gamma\bar{z}e^{j2\Omega\tau} = \Omega_1^2 e^{ja} e^{j\Omega_1\tau} + \gamma(2\Delta e^{j\Omega_1\tau} + \bar{\Delta} e^{j\Omega_2\tau}) \quad (21)$$

The solution for Eq. (21) is given as

$$z = B_1 e^{j\Omega_1\tau} + B_2 e^{j\Omega_2\tau} \quad (22)$$

Substituting Eq.(22) into Eq.(21) and comparing coefficients of each corresponding harmonic term on both sides, the following equations are obtained.

$$\begin{cases} (1-2\gamma-\Omega_1^2+j2\zeta\Omega_1)B_1 - \gamma\bar{B}_2 = \Omega_1^2 e^{ja} + 2\gamma\Delta \\ -\gamma\bar{B}_1 + (1-2\gamma-\Omega_2^2+j2\zeta\Omega_2)B_2 = \gamma\bar{\Delta} \end{cases} \quad (23)$$

The coupled harmonics Ω_1 and Ω_2 appear because of parametric excitation term on left side of Eq. (21). Hence the component Ω_2 is generated regardless of $\Delta=0$, similarly the component Ω_1 is generated even if the unbalance is not present. Figure 8 shows the amplitude of B_1 and B_2 vs. Ω for two cases of $\gamma=0.1$ and $\gamma=0.2$ with respect to $\Delta=1$, $\alpha=0$, $s=0.1$ and $\zeta=0.01$. It is found that B_1 and B_2 become larger as γ increases. And also Fig. 9 shows B_1 and B_2 vs. Ω for two cases of $s=0.05$ and $s=0.1$, while $\gamma=0.1$. Two

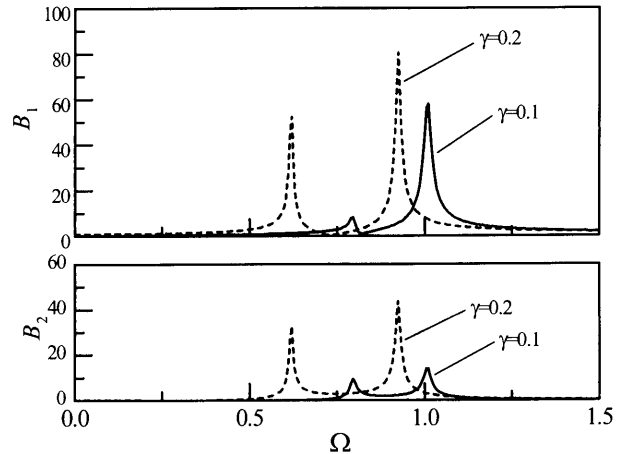


Fig. 8 Response curves of B_1 and B_2 ($\Delta=1$, $\alpha=0$, $s=0.1$, $\zeta=0.01$)

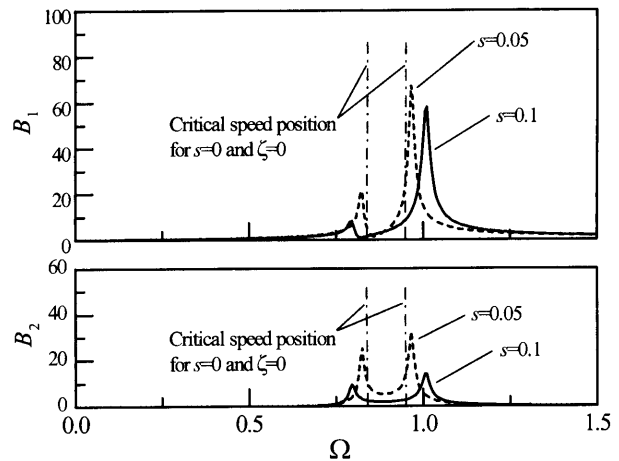


Fig. 9 Response curves of B_1 and B_2 ($\Delta=1$, $\alpha=0$, $\gamma=0.1$, $\zeta=0.01$)

critical speeds⁽⁷⁾ exist in the system with $s=\zeta=0$, such as $\Omega = \sqrt{1-3\gamma}$ and $\Omega = \sqrt{1-\gamma}$. In the case where the slip occurs, there are two critical speeds seen at both sides of the frequency band which incorporates two critical speeds of $s=\zeta=0$ case, and also the magnitude of these two peaks tend to become larger as the slip decreases. A small slip condition that contributes to the slight difference between Ω_1 and Ω_2 may causes beat vibrations.

3.4 Comparison to experimental result

The analytical results of $\gamma=0.1$ case in both Fig. 7 and Fig. 8 are summarized in Fig. 10 as three-dimensional display so that we compare with experimental results as shown in Fig. 2 and Fig. 3. From Fig. 4, the slip ratio is estimated to be 0.1 by taking average of slip ratio values over 50 Hz. The frequency in Fig. 10 is calculated from Eq.(16) by giving $\omega_n = 2\pi \times 82.5$ [rad/s], whereas the amplitude is still dimensionless. There are 2ω , ω_1 and ω_2 components seen in both of

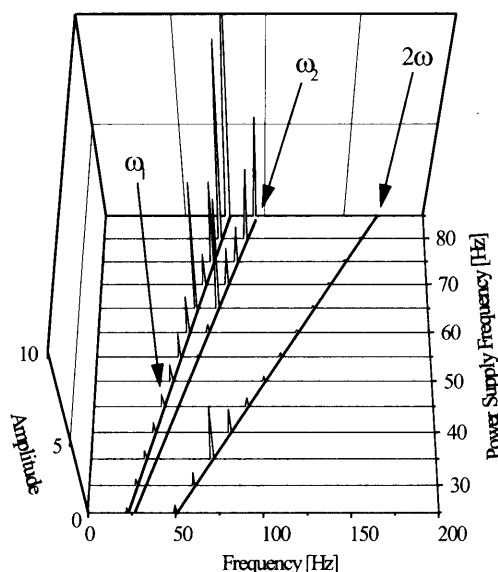


Fig. 10 3D analytical result ($\Delta=1$, $\alpha=0$, $\gamma=0.1$, $s=0.1$, $\zeta=0.01$)

the experimental and the analytical results. It is found from the analysis that 2ω is caused by the offset Z_1 between the stator center and gyrational center of the rotor which is also indicated experimentally by the comparison of Figs. 2 and 3. Although the cause of ω_2 appearance could not be specified in the experiment, it seems analytically to be caused by unbalance and disagreement Δ between gyrational and geometrical center of the rotor. The $2\omega_1$ component was seen in the experiment whereas not in analytical result, which may be because the nonlinearity of the magnetic pull force was not considered in analysis. According to Figs. 2 and 3, the peak of $2\omega_1$ was generated near 40 Hz, which implies that the second harmonic vibration may be excited due to the nonlinearity of the magnetic pull force.

Meanwhile, it was expected that the unstable vibration would occur in the vicinity where the power supply frequency coincides with the natural frequency, however, it did not appear in the present experiment supposedly because the mechanical and the electro-magnetic damping, etc. contributed. Although γ varied in the experiment due to the instability of the current in the stator whereas constant in the analysis, it was found that the analytical investigation qualitatively agrees with the experimental result as to the generation of 2ω , ω_1 and ω_2 .

4. Conclusion

The rotor vibration of two-pole induction motor with rotating magnetic field has been investigated

experimentally and also analytically. The ideal rotating magnetic field was assumed in the analysis, and the vibration characteristics related to the unbalance, the location of gyrational center of the rotor, and the location of geometrical center of the rotor was clarified. Also, the vibration characteristics which was observed in the experiment was verified analytically. The results obtained in this study are summarized as follows.

(1) The 2ω vibration of twice the power supply frequency is generated, which is due to the offset Z_1 between the stator center and the gyrational center of the rotor, and also the magnitude of the vibration is proportional to Z_1 .

(2) Two vibrations, such as $\omega(1-s)$ and $\omega(1+s)$ where s represents slip ratio of rotation are generated. These vibrations are affected by the rotor unbalance and the disagreement Δ between the rotational center and the geometrical center of the rotor, and are also generated for the case either the unbalance or Δ is absent. The vibrations become larger with increase of the unbalance or Δ . Beat vibration may be generated if the slip ratio s is small.

(3) The analytical investigation denotes that the unstable vibration happens to appear when the power supply frequency coincides with natural frequency of the rotor. The unstable vibration did not occur in the experiment because of the damping.

Acknowledgments

The authors would like to thank Mr. K. Ogawa, staff at Kanazawa University for his technical support on producing experimental equipment and Mr. H. Shinagawa and Mr. T. Watanabe for performing experiments.

References

- (1) Watanabe, S., Vibration of Motor, JSME Teaching Material, (in Japanese), Vol. 930, No. 23 (1993), pp. 69-75.
- (2) Kanzaki, H., Sibayama, J., Watanabe, S., Ichimonji, M. and Namiki, M., Unstable Electrical Vibration of an Induction Motor, Trans. Jpn. Soc. Mech. Eng., (in Japanese), Vol. 60, No. 578, C (1994), pp. 3238-3242.
- (3) Edited by JSME Vib. Eng. Workshop, v_Base Data Book, (in Japanese), (1994), pp. 212-213.
- (4) Ref. (3), pp. 214-215.
- (5) Ref. (3), pp. 216-217.
- (6) Yamamoto, T., Mechanical Dynamics, (in Japanese), (1976), pp. 234-241, Asakura-Shoten.
- (7) Gasch, R. and Pfutzner, H., Rotordynamik, (1975), pp. 115-126, Springer-Verlag.